Geophysical Research Letters

RESEARCH LETTER
10.1029/2020GL089325

Poleward Shift of Northern Subtropics in Winter: Time of Emergence of Zonal Versus Regional Signals

Roberta D'Agostino[1], Ascanio Luigi Scambiati[2], Johann Jungclaus[1], and Piero Lionello[2,3]

[1]Max Planck Institute for Meteorology, Hamburg, Germany, [2]DiSTBA, University of Salento, Lecce, Italy, [3]Euro-Mediterranean Center on Climate Change, CMCC, Lecce, Italy

Key Points:
- Recent trends of subtropical margins are not a robust signal of anthropogenic climate change in the Northern Hemisphere
- The internal climate variability prevails over the forced response until 2100 on Northern subtropical margin poleward shift at hemispheric scale
- The poleward shift of Northern subtropics will affect mainly Mediterranean/Middle East and Western Pacific sectors

Supporting Information:
- Supporting Information S1
- Text S1
- Figure S1

Correspondence to:
R. D'Agostino,
roberta.dagostino@mpimet.mpg.de

Citation:
D'Agostino, R., Scambiati, A. L., Jungclaus, J., & Lionello, P. (2020). Poleward shift of northern subtropics in winter: Time of emergence of zonal versus regional signals. *Geophysical Research Letters*, *47*, e2020GL089325. https://doi.org/10.1029/2020GL089325

Received 23 JUL 2020
Accepted 30 AUG 2020
Accepted article online 9 SEP 2020

Author Contributions:
Conceptualization: Roberta D'Agostino, Piero Lionello
Formal analysis: Roberta D'Agostino, Ascanio Luigi Scambiati
Methodology: Roberta D'Agostino, Ascanio Luigi Scambiati
Writing - original draft: Roberta D'Agostino, Ascanio Luigi Scambiati
Writing – review & editing: Roberta D'Agostino, Johann Jungclaus, Piero Lionello

Abstract The Northern Hemisphere mid-latitudes will be exposed to hydroclimatic risk in next coming decades because the subtropical expansion. However, it is not clear when the anthropogenic signal will emerge from the internal climate variability. For this purpose, we investigate the time of emergence (ToE) of the hemispheric and regional shift of northern subtropical margins in the Max Planck Institute Grand Ensemble. For several indicators, the ToE of the poleward shift of Northern subtropical margin will not occur by the end of the 21st century, neither at regional nor at hemispheric scale. The exceptions are the Mediterranean/Middle East and, to a lesser degree, Western Pacific, where the ToE would occur earlier. According to our results, given the fundamental role played by internal variability, trends of Northern Hemisphere subtropical poleward shift that have been identified over last decades in reanalyses cannot be considered as robust signals of anthropogenic climate change.

Plain Language Summary The projected poleward shift of subtropical margins will affect densely populated areas of the Northern Hemisphere that have limited or scarce water resources. Therefore, it is fundamental for societies in these areas to know when the effects of climate change on the regional environment will become evident, because this information can make the difference for effective adaptation and mitigation strategies. The position of the subtropical margins is intimately related to the zonal-mean Hadley Circulation, but is also affected by regional processes related to the distribution of continents, oceans and to their characteristics. In our study we show that the poleward shift of Northern subtropics has strong regional connotations and only in few areas, for example, the Mediterranean/Middle East and, to a lesser extent the Western Pacific, the anthropogenic climate change signal will emerge from the natural climate variability before the end of the 21st century.

1. Introduction

Almost the 40% of Earth's human population lives in subtropical areas that are prone to aridity or desertification in next coming decades. Hence, investigating the magnitude and the rate of Northern subtropical margin shift is fundamentally important for water availability and environmental and societal changes (Doxsey-Whitfield et al., 2015; Heffernan, 2016).

Subtropical climate is characterized by lack of clouds, rainfall scarcity, transition from positive-to-negative surface moisture budget, subsidence, and high surface pressure, characteristics associated with the descending branch of the Hadley Circulation (HC). Several studies have leveraged on this link for developing indicators to investigate changes of HC width and poleward shift of its subtropical margins (Adam et al., 2018; Chen et al., 2014; Davis & Davis, 2018; Nguyen et al., 2018; Schwendike et al., 2014; Staten et al., 2018).

Recent literature emphasized how magnitude and significance of the HC poleward shift and tropical width expansion from 1979 onward disagree among studies: Rates are ranging from few tenths to several degrees latitude per decade, and they are not always significant (Davis & Birner, 2017; D'Agostino & Lionello, 2017; Hu & Fu, 2007; Nguyen et al., 2015; Staten et al., 2018). Differences among these studies have been attributed to observational uncertainties, reanalyses and models used, the considered time period and seasons, as well as the variety of indicators used to quantify poleward shift rates (Waugh et al., 2018). In particular, a considerable fraction of uncertainty has been attributed to the use of some indicators, poorly covarying with zonal-mean mass stream function (the traditional metric used to represent the HC extent) and showing, additionally, unsatisfactory correlations among themselves (Waugh et al., 2018).

Beyond that, the influence of natural/internal climate variability has been highlighted to be a source of discrepancy on zonal-mean HC trends in last decades (D'Agostino & Lionello, 2017; Grise et al., 2018, 2019; Kang et al., 2013; Staten et al., 2018). In fact, when accounting for different indicators to estimate HC edges, CMIP5 simulations show that most of recent trends in reanalyses do not exceed the range of natural variability in global climate models, because the length of the observational record over the satellite era (30–40 years) is simply too short to detect any anthropogenically forced signal (Grise et al., 2018; Staten et al., 2018). In particular in the Northern Hemisphere, CMIP5 simulations indicate that the anthropogenic greenhouse gas (GHG) increase contributed to a very small poleward shift of zonal-mean HC edges, and such a small forced signal is only detectable using a large ensemble of model simulations. At regional scale, the forced responses to individual forcing (e.g., GHG increase, stratospheric ozone depletion, and anthropogenic aerosols) is difficult to quantify because the natural variability has a large impact (Staten et al., 2018), in particular because the GHG-induced HC poleward shift might be counteracted by the presence of aerosols. These aspects leave room for discussion about where the anthropogenic forcing, especially the CO_2, will affect more the subtropical shift and HC expansion.

Additionally, it is unclear when the forced poleward shift of the HC will possibly emerge from the internal climate variability. A recent study on the Community Earth System Model Large Ensemble (CESM-LE), a global climate model composed of 40-ensemble members for the period 1920–2100 forced with Historical and RCP8.5 forcing, shows that two indicators used to identify HC edges (i.e., the zonal-mean mass streamfunction and the surface wind changes) indicate that the forced signal will not emerge from the noise during the 21st century in the Northern Hemisphere (Grise et al., 2019). However, as the time of emergence (ToE, i.e., the year when the signal emerges from the noise) is intrinsically related to some thresholds, results might vary among indicators, data sets, and regions.

Here, we quantify the relative role of the internal climate variability against the external forcing in the Max Planck Institute-Grand Ensemble (MPI-GE) (Bittner et al., 2016; Maher et al., 2019; Stevens, 2015) on the shift of Northern subtropical margin. We extend our investigation beyond the study by Grise et al. (2019), analyzing the ToE at hemispheric (zonal average) and at regional scale using six indicators for detecting subtropical margins, in order to identify the areas most sensitive to the anthropogenic forcing. The regional approach is an aspect never investigated before. Furthermore, we have considered the 1%CO_2 experiment, for an improved characterization of the ToE related to CO_2-only forcing. We introduce the MPI-GE and the indicators used for the analysis in section 2, then we first analyze the latitudes, trends, and ToE of zonally averaged indicators (section 3.1), and afterward the regional characteristics of subtropical margins (section 3.2). We summarize and conclude the paper (section 4).

2. Data and Methods

The MPI-GE is currently the largest ensemble available among the climate models (Bittner et al., 2016; Giorgetta et al., 2013; Maher et al., 2019; Stevens, 2015). It consists of the ocean component, MPIOM (Jungclaus et al., 2013), the ocean biogeochemistry model HAMOCC 5.2 (Ilyina et al., 2013), the atmospheric model ECHAM (Stevens et al., 2013) coupled to the land component, JSBACH, which includes land use transition with the standard fire module, and interactive vegetation (Reick et al., 2013). The atmospheric model resolution is 1.875° (T63L47) and the ocean model is on GR15L40 grid, featuring a horizontal resolution between 22 and 220 km and 40 vertical levels. For in-depth details refer to Maher et al. (2019).

In this study, we have investigated the evolution of subtropical margins in the Historical simulation (1850–2005) and in two other climate experiments, the RCP8.5 until the end of the 21st century and the 1%CO_2 (150 years). We use these three experiments to explore the sensitivity of our results to different forcing. The comparison between RCP8.5 and 1%CO_2 ensures that the evolution of the subtropical margins cannot be attributed to aerosols, other GHG gases (such as ozone) or land use changes in the subtropical regions.

We focus the analysis on boreal winter (December-to-February, DJF), when hydroclimate conditions of some densely populated areas (e.g., Mediterranean and California) at the Northern side of subtropics are particularly sensitive to storm track position (Mariotti et al., 2002; Seager, Liu, et al., 2014; Seager, Neelin, et al., 2014), to HC expansion and/or poleward shift of subtropical margins (Seager et al., 2010) and hence

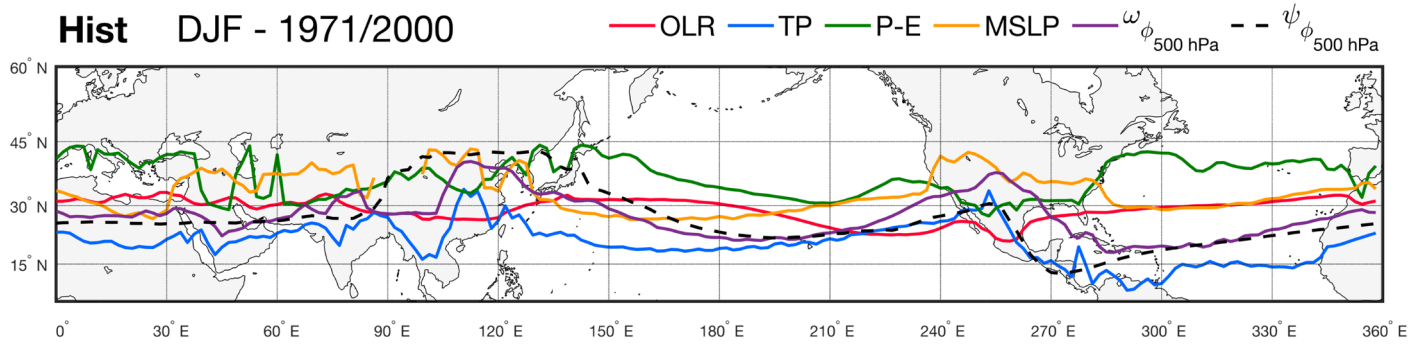

Figure 1. Northern subtropical margins computed using OLR (red), TP (blue), P-E (green), MSLP (yellow), ω_{ϕ} (purple), and ψ_{ϕ} (dashed black) at 500 hPa. Lines show the average wintertime (DJF) position in the period 1971–2000 of the Historical experiment.

more impacted by water scarcity. Furthermore, the Northern HC is strongest and well defined in DJF; therefore, it is possible to detect easily the regional position of its edges.

The latitude of the subtropical margins is computed by using six different indicators. Some of them are related to precipitation, which has relevant implications for society, and some of them have been already used in past studies as indicators of the position of the HC edges:

- OLR (outgoing longwave radiation): poleward-most latitudes where OLR falls below 250 W/m^2 (Adam et al., 2018; Chen & Bordoni, 2014; Davis & Davis, 2018; Davis & Rosenlof, 2012; Hu & Fu, 2007; Johanson & Fu, 2009). It is associated with the absence of clouds in the subtropics.
- TP (total precipitation): latitudes of absolute precipitation minima in the subtropics (Chen & Bordoni, 2014; Chen et al., 2014; Hu & Zhou, 2010). It describes rainfall scarcity.
- P-E (precipitation-evaporation): zero-crossing latitudes of P-E (Adam et al., 2018; Davis & Birner, 2016; Davis & Davis, 2018; Davis & Rosenlof, 2012; Johanson & Fu, 2009; Lu et al., 2007; Staten et al., 2018), associated with the dry conditions and negative surface water balance in the subtropics.
- MSLP (mean sea level pressure): latitudes of absolute maxima of the MSLP (i.e., high-pressure ridges in the subtropics) (Adam et al., 2018; Davis & Davis, 2018; Hu & Zhou, 2010).
- ω_{ϕ} (vertical velocity associated with the meridional overturning circulation or, in other words, the vertical velocity associated with the meridional component of the divergent wind): latitudes of absolute maxima near the subsiding branches at 500 hPa (Schwendike et al., 2014, 2015). It describes the subsidence in the subtropics.
- ψ_{ϕ} (streamfunction of the regional meridional overturning circulation): zero-crossing latitudes of ψ_{ϕ} at 500 hPa (Nguyen et al., 2018; Schwendike et al., 2014), associated with the poleward limit of the HC in the subtropics.

Regional subtropical margins are computed for all indicators and at each longitude within the 5°–45°N range, as shown in Figure 1.

Recently, it has been emphasised that the regionality of the tropical atmospheric circulation depends also on the zonal component of the mean flow in some areas. This implies that the edge definition might be affected by the zonal flow too, as in the Pacific around 170°W (Raiter et al., 2020). The use of the indicators based on precipitation, surface pressure, and OLR and the degree of agreement they have with ω_{ϕ} and ψ_{ϕ} serves to avoid any ambiguity on results by using different definition of subtropical margins. In particular, we have noticed that most of the discrepancy between different indicators occurs over the Pacific and Atlantic ocean: These might be the areas where the mean atmospheric flow has the largest zonal component in DJF (Figure 1). However, since we are more interested in the societal implication of subtropical margin shift on regional hydroclimate, we will analyze in detail only results over the continents.

The impact of the external forcing is described by the so-called forced response F^i_{fr}, represented by the mean of all ensemble members f^i_e, where $e = 1, \ldots, 100$, represents the ensemble member and i represents the time step. The total variance of the ensemble TV is decomposed in the variance of the forced response FV and in the internal variance IV (Bellomo et al., 2018; Maher et al., 2019). FV is the variance associated with the

evolution of the forced response (described by the ensemble mean), while *IV* is the variance associated to the overall variability of the ensemble members relative to the ensemble mean:

$$TV = FV + IV \text{ and } \sigma_{TV}^2 = \sigma_{FV}^2 + \sigma_{IV}^2. \quad (1)$$

Here, σ_{TV}, σ_{FV}, and σ_{IV} denote the square root of *TV*, *FV*, *IV*, respectively, and represent the total uncertainty of the signal and its components (see the supporting information for the algebraic expressions).

The methods for estimating the signal-to-noise ratio *S*/*N*, which is needed for computing the ToE, differ among studies (Christensen et al., 2007; Deser et al., 2016; Giorgi & Bi, 2009; Hawkins & Sutton, 2012). Here, the signal S_j at time t_j is given by the anomaly of the 31-year running mean $\overline{(\cdot)}_j$, centered at time t_j, of the ensemble mean position F_{fr}^i of the subtropical margin with respect to its value in the reference period $F_{fr\ (1971-2000)}^{ref}$, as $S_j = \overline{(F_{fr})}_j - F_{fr}^{ref}$. The noise N_j is estimated as the standard deviation associated with the internal climate variability σ_{IV} at each time step (t), considering 31-year-long time windows, centered at t_j. The value of the ToE is computed as the year when *S*/*N* crosses the 0.5 or 1 threshold. In aforementioned studies (Grise et al., 2019; Staten et al., 2019), the noise has been estimated using the internal climate variability in the reference period. In our case, we considered its possible variation with time. However, we found that this variation turns out to be negligible. We have estimated the *S*/*N* ratio and the corresponding ToE for each ensemble member. In this case, the signal is computed as the anomaly of the 31-year running mean with respect to the 1971–2000 mean and the noise *N* as the standard deviation in the reference period, 1971–2000. The best estimate of the ToE is the median of the members' ToEs. The 5th to 95th percentiles of the distribution are used to delimit its uncertainty range.

At regional scale, a slightly different method is applied. The regional signal is linearly approximated using its trend (computed using the whole duration of the experiment): $S(\lambda, t) \approx \partial F_{fr}(\lambda, t)/\partial t|_{Exp}(t - t_0)$. The index *Exp* indicates the experiment (in turn Historical, 1%CO_2, RCP8.5) that is used for computing the trend and t_0 the corresponding initial time. The noise $\sigma_{IV\,(\lambda)}|_{Exp}$ is the standard deviation of the regional *IV*, which is a function of the longitude. The signal-to-noise ratio is then approximated as follows:

$$\frac{S(\lambda, t)}{N(\lambda)} \approx \frac{\partial F_{fr}(\lambda, t)/\partial t|_{Exp}}{\sigma_{IV(\lambda)}|_{Exp}} \cdot (t - t_0). \quad (2)$$

This allows to estimate the time *t* needed to reach an established signal-to-noise ratio threshold, which is the ToE in terms of years after the initial date of each experiment.

3. Results

3.1. Zonally Averaged Northern Subtropical Margins: Uncertainty in the Latitude, Trends, and ToE

The latitude of the Northern subtropical margins strongly depends on the adopted indicator (Figure 1), with P-E and TP delimiting the most poleward and equatorward margins, respectively. For all indicators and in every experiment, most of the uncertainty in the latitude of the zonally averaged subtropical margins is due to the internal climate variability (*ICV*; Figure 2, left panels, diamonds). The unique exception is OLR, which exhibits a large sensitivity to the 1%CO_2 forcing (*FV*, stars), with the forced response accounting for 30% of the total variance (*TV*, dots). In fact, for all other indicators, the contribution of the forced response to the total variance is small or even negligible, ranging from a minimum 1% for P-E and MSLP in the Historical to a maximum 13% for MSLP in the 1%CO_2. In spite of the large ensemble spread, for all indicators the ensemble mean of Northern subtropical margins exhibit a consistent poleward shift, which progressively increases with time in the 1%CO_2 and the RCP8.5 experiments (see Figure S1).

The magnitude of the trends of the ensemble mean (forced trends; Figure 2, right panels) depends on the indicator too, varying in the range from 0.04° per decade for TP in the 1%CO_2 experiment to 0.12° per decade for MSLP in the RCP8.5. Conversely, trends are small and uncertain in the Historical. Though the 1%CO_2 and RCP8.5 forced trends are always positive and statistical significant, individual members exhibit much uncertain trends (Figure 2, right panels). Most of the ensemble members of the 1%CO_2 show trends that

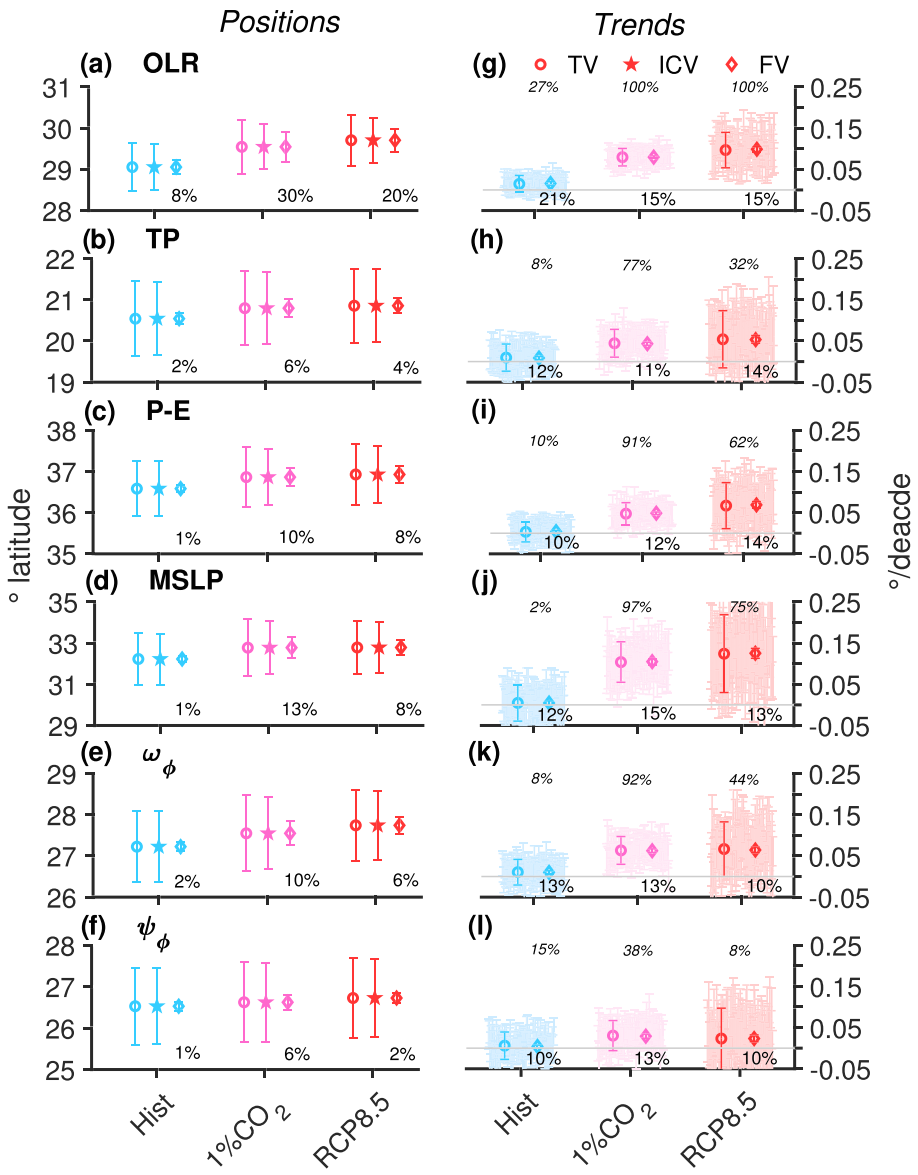

Figure 2. Positions and trends of the zonally averaged Northern subtropical margins and corresponding uncertainties for the Historical (blue), 1%CO_2 (pink) and RCP8.5 (red). Symbols denote total (dots), forced (diamond), and internal (stars) uncertainties (see Equation 1). The associated error bars show the corresponding 5th to 95th confidence range. Left panels show the mean value of the time series (see Figure S1) over the whole period of the experiments. Annotated percentages show the ratio of the forced variance to the total variance. Right panels show the value of the trends (Sen's slopes) considering the whole length of the simulations. Pale colors (light blue, pink, and red) denote the uncertainty ranges of the trends of the ensemble members. Annotated values are the percentage of the forced to the total variance (normal font along the bottom axis) and the fraction of members with a statistically significant positive trend (Mann-Kendall test, 95% confidence level, italic font on top of panels).

are sufficiently large to be statistically significant, while RCP8.5 trends are often not significant for several indicators (namely, TP, ω_ϕ, and ψ_ϕ). The percentages annotated in the right panels of Figure 2 can be interpreted as probability of detecting a significant trend and are larger than 90% for most indicators only in the 1%CO_2.

Summarizing, the poleward shift of Northern subtropics appears to be robust and significant across the different indicators, and it will increase as the climate warms. However, the forced shift emerges from the internal variability only if the signal is sufficiently large. The early signals in the Historical are too small for

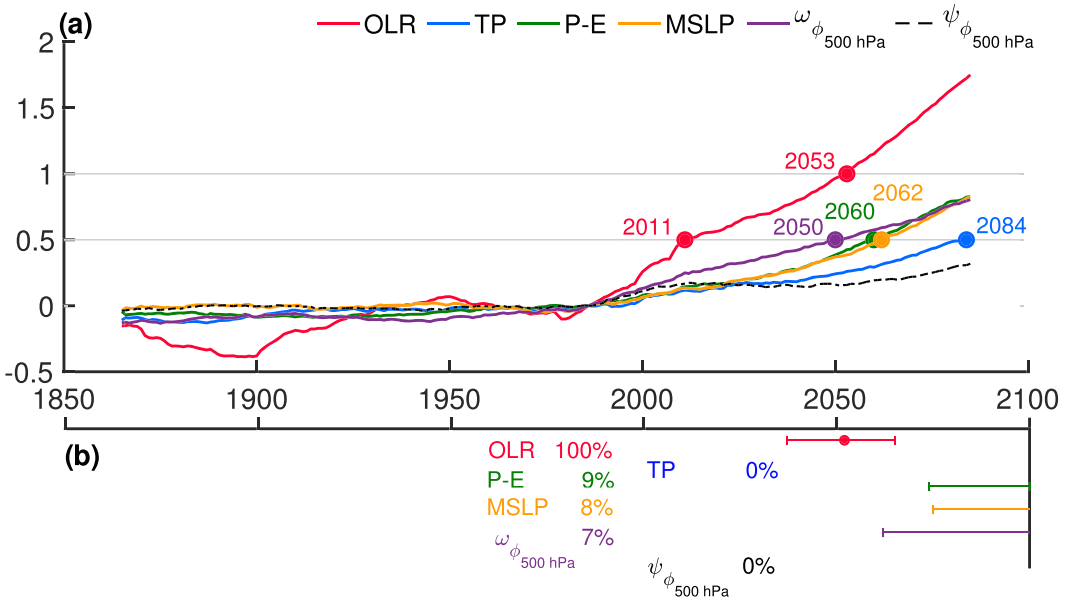

Figure 3. Time of emergence (ToE) of the zonally averaged Northern subtropical margins' shift. Top panel shows the time series of the signal-to-noise ratio S/N of the ensemble mean for different indicators: OLR (red), TP (blue), P-E (green), MSLP (brown), ω_{ϕ} (purple), and ψ_{ϕ} (dashed black) at 500 hPa. Time series are obtained joining the Historical and RCP8.5 experiments and consider the 1865–2085 period along which the 31-year running mean is available. Grey horizontal lines mark the $S/N = 0.5$ and 1.0 thresholds. Bottom panel shows the median ToE of the 100 ensemble members with bars representing the range of the distribution (5th to 95th percentile). The percentage of members with ToE occurring within the end of the 21st century is annotated in the panel. When this percentage is smaller than 50% (95%) the median (the 95th percentile) cannot be computed and the range would fall outside the time period shown in the figure.

allowing their detection and attribution to the anthropogenic forcing. In the RCP8.5 signals are larger than in the Historical, but in any case for TP, ω_{ϕ} and ψ_{ϕ} the probability of detecting a significant trend is lower than 50%. Therefore, the probability of detecting a significant trend of the subtropical margins during the 21st century is low.

The comparatively large internal variability has important consequences on the ToE of the Northern subtropical margin's shift. Figure 3 shows the evolution of S/N (signal-to-noise ratio) for all indicators considering the time series built by joining the Historical and RCP8.5. If the threshold $S/N = 1$ is adopted for the ToE, only OLR provides a ToE within the 21st century (around 2050). If a much lower threshold $S/N = 0.5$ is considered, ToE is anticipated to 2011 for OLR and shifts to 2050, 2060, 2062, and 2084 for ω_{ϕ}, P–E, MSLP, and TP, respectively, while for ψ_{ϕ} it does not occur within the considered time range. Results are substantially equivalent if ToE is estimated separately for each member. The median values with the corresponding 5th to 95th uncertainty bars are shown in Figure 3b. Here we considered the threshold $S/N = 1$. Only OLR and P-E estimate the occurrence of ToE within this century at the 95th confidence level. Note that the adopted methodology actually prevents to detect ToE occurring beyond 2085.

Therefore, though the anthropogenic climate change will certainly cause the poleward shift of the Northern subtropical margin, it is unlikely that the signal will emerge from the natural variability within the 21st century (more precisely before the last decade of the 21st century) at hemispheric scale.

3.2. Regional Subtropical Margins: Uncertainty in the Latitudes, Trends, and ToE

The latitudes of regional subtropical margins in the Northern Hemisphere (Figure 1) are far from being zonally uniform. Regional features, which are usually hidden by taking the zonal average, exhibit large differences among indicators.

The OLR shows the smallest zonal variations, with northward deviations in areas free of clouds, such as the Mediterranean and the Western Pacific, and southward deviations in correspondence with cloudy areas above Indochina, North America and Eastern Pacific. The subtropical margins detected by ω_{ϕ} and ψ_{ϕ}, which

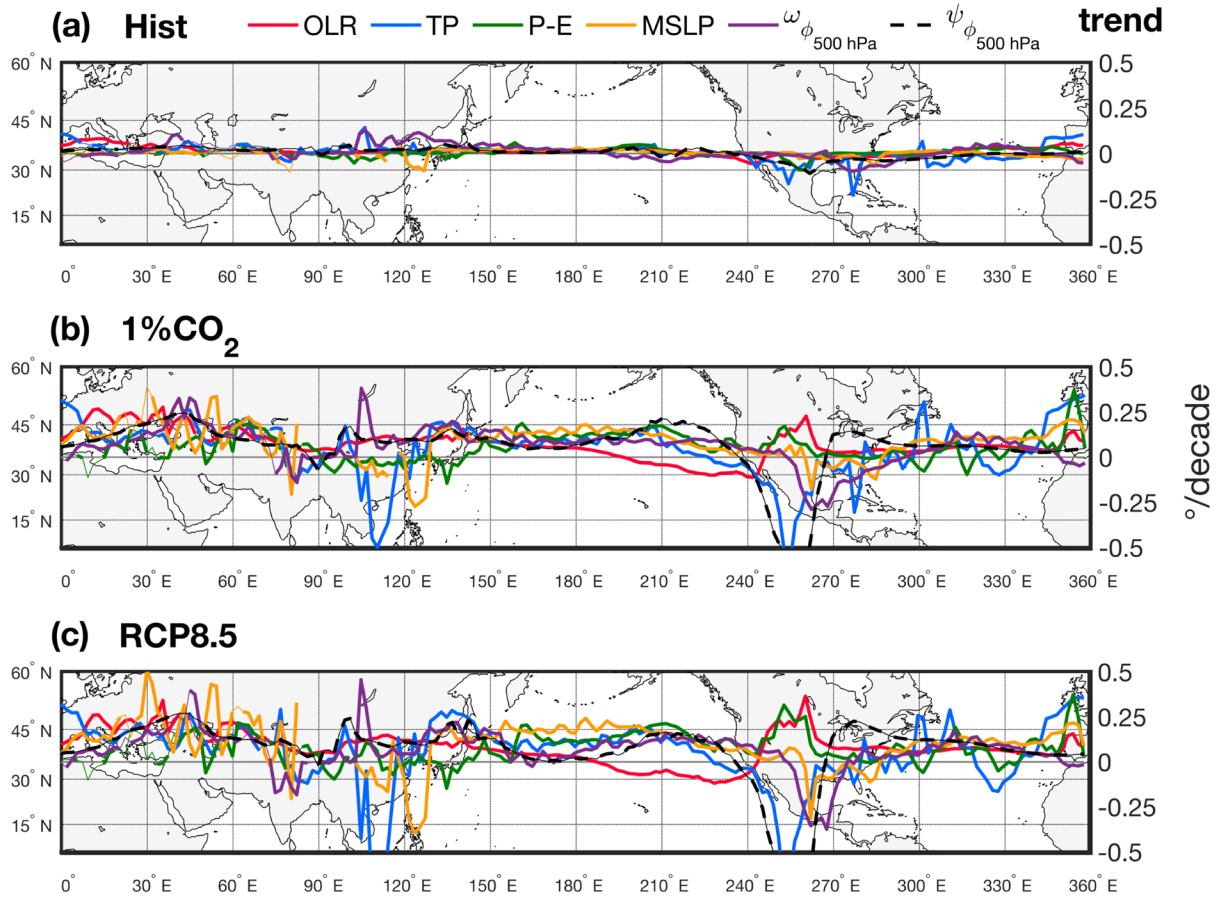

Figure 4. Regional values of the ensemble mean trend (units degrees per decade) for the three different experiments: Historical (top), 1%CO_2 (middle), and RCP8.5 (bottom). Indicators are shown by colored lines: OLR (red), TP (blue), P-E (green), MSLP (brown), ω_{ϕ} (purple), and ψ_{ϕ} (dashed black). Bold parts of the lines indicate the regions where the trend is significant at the 95% level according to the Mann-Kendall test.

are by definition two indicators directly related to the atmospheric circulation, have rather similar positions above the oceans and flat areas, but they differ in the presence of strong orography (e.g., Himalaya, Tibetan Plateau, Rocky Mountains, and Central America). The MSLP systematically deviates northward above continents because of the presence of the Siberian High and the high-pressure systems above North America in winter. There is a clear systematic deviation between the regional and zonal averaged positions of the precipitation minima (TP) and ω_{ϕ} maxima. The former are always southward of the latter because lack of moisture in the atmosphere southward of the ω_{ϕ} maxima is likely to be a key factor determining precipitation minima. The P-E locates the margins systematically north of the precipitation minima (TP) because it includes the effect of evaporation. This effect is large above oceans, particularly over their warm pools. The effect of the Mediterranean Sea is evident as well. These results stress the importance of different regional features on the positions of the subtropical margins provided by different indicators.

Also regional trends are not zonally uniform and differ among indicators (Figure 4). Differences are particularly large above Indochina and North America, where some indicators show equatorward trends instead. Considering a single indicator, its trend has a similar regional behavior in the three experiments, but its magnitude is largest in the RCP8.5 and smallest in the Historical. In spite of the spatially irregular behavior of the trends, some regions provide trends with a consistent positive sign with a similar magnitude: Mediterranean/Middle East and Western Pacific.

Figure 5 shows the trend of the signal-to-noise ratio $S/N = \dfrac{\partial F_{fr}(\lambda,\, t)/\partial t|_{Exp}}{\sigma_{IV(\lambda)}|_{Exp}}$ (see Equation 2). This figure allows to identify the regions where the anthropogenic poleward shift of the Northern subtropics will emerge from the noise before the end of the 21st century. In this figure the thresholds 0.1 and 0.25 are marked with

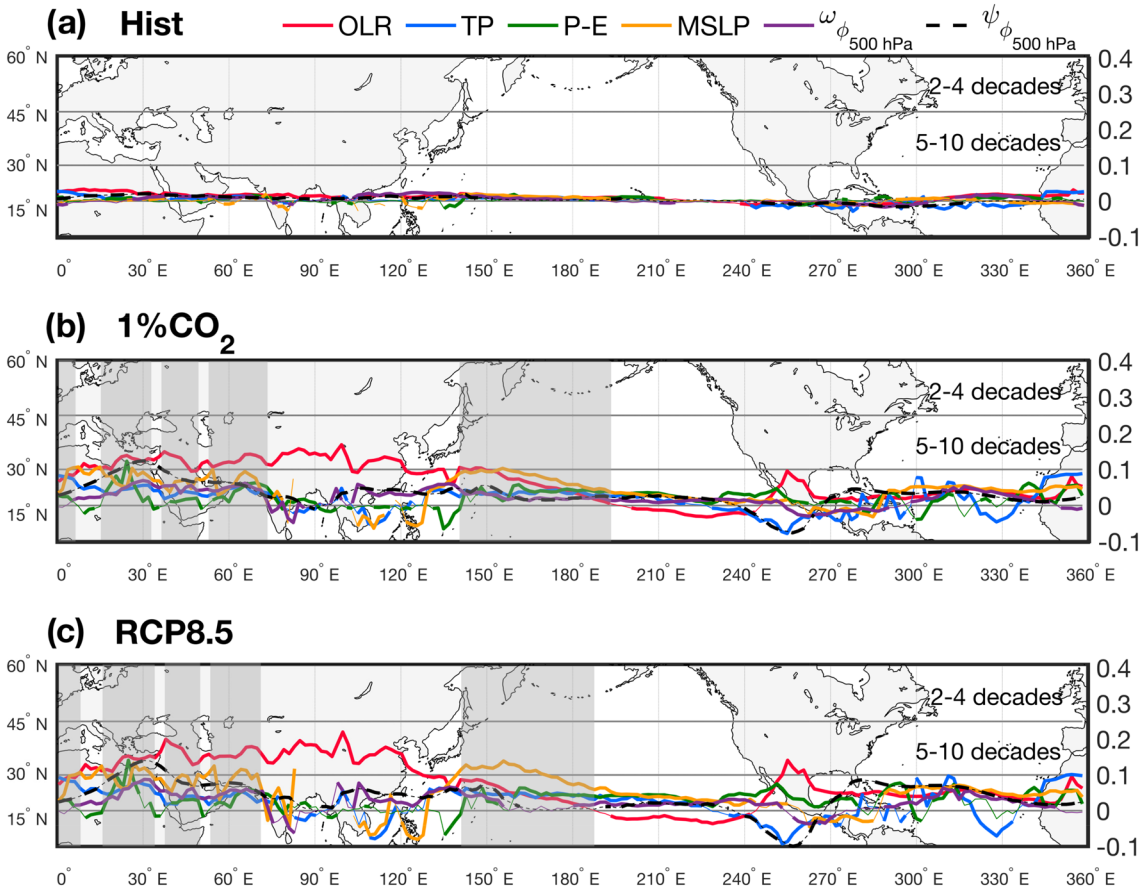

Figure 5. Regional values of the trend of the signal-to-noise ratio $S/N = \frac{\partial F_{fr}(\lambda, t)/\partial t|_{Exp}}{\sigma_{IV(\lambda)}|_{Exp}}$ (per decade; see Equation 2). Each panel shows values for different indicators, for example, OLR (red), TP (blue), P-E (green), MSLP (brown), ω_ϕ (purple), and ψ_ϕ (dashed black) at 500 hPa for Historical (top), 1%CO_2 (middle), and RCP8.5 (bottom). The bold parts of the curves indicate the regions where the trend is significant at the 95% level according to the Mann-Kendall test. For values of the trends above the 0.25 and 0.1 grey horizontal lines, the signal will exceed the noise in four decades and in one century, respectively. Grey shaded areas show regions where all indicators agree on the positive S/N.

grey horizontal lines. For values of the trends above the 0.1, the signal will exceed the noise in one century. If a weaker criterion $S/N = 0.5$ is assumed, the trend the detection would occur in five decades. The threshold 0.25 denotes the level required for the signal exceeding the noise in four decades. In the Historical, trends are extremely small and their rate of change is everywhere far from the level that would allow its detection within the 21st century. However, the past rate of change is expected to accelerate in the future: RCP8.5 and 1%CO_2 present in fact larger values than the Historical. RCP8.5 and 1%CO_2 shows that the ToE of the poleward shift of Northern subtropics is not regionally uniform as well. For many indicators, the ToE will occur sooner over Mediterranean/Middle East and Western Pacific (see grey areas in Figure 5), while the large effect of internal climate variability prevents the ToE within the 21st century above the Eastern Pacific.

Regional processes, such as changes of available moisture provided by atmospheric advection, can explain the differences in trends among the indicators shown in Figure 4. The OLR presents large northward trends of subtropical margins over North America and the Mediterranean, where climate projections suggest increased aridity and cloudless conditions as consequence of reduced moisture mean transport (D'Agostino & Lionello, 2020; Seager et al., 2007). In particular, over North America, the northward trend of OLR disagrees with the southward trends provided by ψ_ϕ and ω_ϕ (direct indicators of the position of the HC descending branch) and by TP (the latitude of the precipitation minima). TP exhibits also a large southward trend of the subtropics over Eastern Asia, consistently with a future increased precipitation over China (Tian et al., 2015). The TP behavior is possibly explained by an increased northerly moisture transport (Ma et al., 2012), caused by the southward shift of the subtropical highs over the Chinese sea, a feature also

shown by the MSLP indicator. Furthermore, the OLR presents a southward trend over the Eastern Pacific, where the low-stratus clouds are projected to decrease over the cool southward branch of the subtropical gyre (Su et al., 2014), while other indicators do not show any trend in this specific area. The disagreements discussed above shows the relevance of regional processes when comparing different indicators. Lack of consensus prevents from getting a robust conclusion for several regions and is the consequence of the complicated conditions in the subtropics, which cannot be attributed uniquely to the descending branch of the HC. The agreement among indicators over Mediterranean/Middle East suggests that these regions will be future hot spots, with a more evident poleward shift of the subtropics than in the rest of the Northern Hemisphere.

4. Summary and Conclusion

In the past decades several studies have investigated the poleward shift of the subtropical belt. These studies were mostly focused on the HC expansion and on the suitability of different indicators to detect its shift. Disagreements among studies have been attributed to differences among indicators, data sets, and, recently, to the role of internal climate variability.

In this study we have focused on the distinction between zonal average and regional poleward shift of Northern Hemisphere subtropical margins, using indicators associated with the characteristics of the subtropical belt, such as lack of clouds (OLR), rainfall scarcity (TP), transition from positive-to-negative surface moisture budget (P-E), subsidence, and high surface pressure (ω_ϕ, MSLP). We have further included, as a reference, the meridional mass stream function (ψ_ϕ), computed by meridional divergent winds, which is the most common metric used for studies of the HC extent. The role of internal variability versus the forced response on regional subtropical shifts has been investigated in the MPI-GE. By design, the MPI-GE allows to disentangle the role of internal climate variability and forced response in the full phase space of both the ocean and the atmosphere states. Furthermore, in order to detect the sensitivity of our results to different concentration of GHG, we have used three different experiments from the MPI-GE: the Historical, the RCP8.5 and 1%CO_2. We have considered the winter season when the subtropical shift strongly affects the water cycle of the Northern Hemisphere arid and semiarid areas, for which is extremely important estimating the regional ToE for triggering adaptation measures.

For all indicators and in all experiments, the uncertainty on the latitude of subtropical margins is predominately affected by the internal climate variability. If OLR is excluded, in the Historical experiment the forced response has a negligible role on the total variance of the subtropical margins (never exceeding 2%). The contribution of the forced response remains small also in the RCP8.5 (2006–2099) and in the presence of nonlinear increment of CO_2 (1%CO_2 simulation). Similarly, uncertainty on trends are caused by large internal variability, with the effect of forced response never exceeding 15% of the total trend variance.

Different indicators produce different future rates of Northern subtropics' shift at hemispheric and regional scale. The disagreement among the regions where regional shifts are detected suggests that these indicators reflect changes produced by the anthropogenic climate change on regional processes. The forced response is more important for OLR than for all other indicators. OLR trends depend directly on thermodynamics, atmospheric moisture, and cloud distributions, and this explains its large sensitivity to anthropogenic climate change and its differences with respect to other indicators (Adam et al., 2018; Waugh et al., 2018). Regional and local processes affect also the indicators based on precipitation, evaporation, MSLP, and vertical velocity fields, but their effect on OLR is so strong that its behavior should be cautiously considered to be representative of the shift of subtropical margins and of the HC expansion (Waugh et al., 2018).

Some previous studies attributed past observed poleward shift signals of the Northern subtropics to global warming (D'Agostino et al., 2017; Liu et al., 2012; Lu et al., 2007; Nguyen et al., 2013). However, due to the large influence of the internal variability, the forced response of the Northern subtropical margin shift in winter will not emerge at hemispheric scale before the end of the 21st, both in MPI-GE (as shown here) and in CESM-LE (Grise et al., 2019). Therefore, trends associated with a poleward shift of Northern subtropics observed in reanalyses over last decades, especially those based on the meridional mass stream function, cannot be considered a robust signal of anthropogenic forcing. On one hand, our results confirm that anthropogenic climate change will produce a poleward shift of the Northern Hemisphere subtropical margins but,

on the other hand, suggest that a robust detection of an anthropogenically induced signal at hemispheric scale is unlikely within the 21st century. The latter conclusion is in contrast with the wide literature on reanalysis data and CMIP3 and CMIP5 models, as already pointed out in the analysis of the CESM-LE ensemble (Grise et al., 2019).

Disagreement among studies that have investigated past trends in observational data sets and reanalyses can be explained by their attempt to assess a signal that is too small to be detectable. Their results reflect mainly multidecadal fluctuations, as pointed out by (D'Agostino & Lionello, 2017) and not a sustained long-term climate trend. However, at regional scale, there are some areas particularly exposed to the subtropical northward shift: Mediterranean/Middle East and Western Pacific. A combination of factors, such as lack of precipitation, negative surface water budget, persisting subsidence and anticyclones characterize these areas as an hot spot of future climate change. In such areas, all indicators agree on a significant northward shift of subtropics, producing a signal that will be detectable within the end of the 21st century.

Data Availability Statement

The MPI-GE data that have been used in this study are available at esgf-data.dkrz.de/projects/mpi-ge/ and can be freely downloaded after having signed the data-use license.

Acknowledgments
Roberta D'Agostino was funded by JPI-Belmont Forum project PaCMEDy, Palaeoclimate Constraints on Monsoon Evolution and Dynamics, and CLICCS Cluster of Excellence, Hamburg, A4-Asian, and African monsoon margins.

References

Adam, O., Grise, K. M., Staten, P., Simpson, I. R., Davis, S. M., Davis, N. A., et al. (2018). The TropD software package (v1): Standardized methods for calculating tropical-width diagnostics. *Geoscientific Model Development*, *11*(10), 4339–4357. https://doi.org/10.5194/gmd-11-4339-2018

Bellomo, K., Murphy, L. N., Cane, M. A., Clement, A. C., & Polvani, L. M. (2018). Historical forcings as main drivers of the Atlantic multidecadal variability in the CESM large ensemble. *Climate Dynamics*, *50*(9-10), 3687–3698.

Bittner, M., Schmidt, H., Timmreck, C., & Sienz, F. (2016). Using a large ensemble of simulations to assess the northern hemisphere stratospheric dynamical response to tropical volcanic eruptions and its uncertainty. *Geophysical Research Letters*, *43*, 9324–9332. https://doi.org/10.1002/2016GL070587

Chen, J., & Bordoni, S. (2014). Orographic effects of the Tibetan Plateau on the East Asian summer monsoon: An energetic perspective. *Journal of Climate*, *27*(8), 3052–3072.

Chen, S., Wei, K., Chen, W., & Song, L. (2014). Regional changes in the annual mean Hadley circulation in recent decades. *Journal of Geophysical Research: Atmospheres*, *119*, 7815–7832. https://doi.org/10.1002/2014JD021540

Christensen, J. H., Hewitson, B., Busuioc, A., Chen, A., Gao, X., Held, R., et al. (2007). Regional climate projections. In *Climate change, 2007: The physical science basis. contribution of Working Group I to the Fourth Assessment Report of the Intergovernmental Panel on Climate Change* (Chap. 11, pp. 847–940). Cambridge: Cambridge University Press.

D'Agostino, R., & Lionello, P. (2017). Evidence of global warming impact on the evolution of the Hadley Circulation in ECMWF centennial reanalyses. *Climate Dynamics*, *48*(9-10), 3047–3060. https://doi.org/10.1007/s00382-016-3250-0

D'Agostino, R., & Lionello, P. (2020). The atmospheric moisture budget in the Mediterranean: Mechanisms for seasonal changes in the Last Glacial Maximum and future warming scenario. *Quaternary Science Reviews*, *241*, 106392. https://doi.org/10.1016/j.quascirev.2020.106392

D'Agostino, R., Lionello, P., Adam, O., & Schneider, T. (2017). Factors controlling Hadley circulation changes from the Last Glacial Maximum to the end of the 21st century. *Geophysical Research Letters*, *44*, 8585–8591. https://doi.org/10.1002/2017GL074533

Davis, N., & Birner, T. (2016). Climate model biases in the width of the tropical belt. *Journal of Climate*, *29*(5), 1935–1954.

Davis, N., & Birner, T. (2017). On the discrepancies in tropical belt expansion between reanalyses and climate models and among tropical belt width metrics. *Journal of Climate*, *30*(4), 1211–1231.

Davis, N. A., & Davis, S. M. (2018). Reconciling Hadley Cell expansion trend estimates in reanalyses. *Geophysical Research Letters*, *45*, 11,439–11,446. https://doi.org/10.1029/2018GL079593

Davis, S. M., & Rosenlof, K. H. (2012). A multidiagnostic intercomparison of tropical-width time series using reanalyses and satellite observations. *Journal of Climate*, *25*(4), 1061–1078.

Deser, C., Terray, L., & Phillips, A. S. (2016). Forced and internal components of winter air temperature trends over North America during the past 50 years: Mechanisms and implications. *Journal of Climate*, *29*(6), 2237–2258.

Doxsey-Whitfield, E., MacManus, K., Adamo, S. B., Pistolesi, L., Squires, J., Borkovska, O., & Baptista, S. R. (2015). Taking advantage of the improved availability of census data: A first look at the gridded population of the world, version 4. *Papers in Applied Geography*, *1*(3), 226–234.

Giorgetta, M. A., Jungclaus, J., Reick, C. H., Legutke, S., Bader, J., Böttinger, M., et al. (2013). Climate and carbon cycle changes from 1850 to 2100 in MPI-ESM simulations for the Coupled Model Intercomparison Project phase 5. *Journal of Advances in Modeling Earth Systems*, *5*, 572–597. https://doi.org/10.1002/jame.20038

Giorgi, F., & Bi, X. (2009). Time of emergence (ToE) of GHG-forced precipitation change hot-spots. *Geophysical Research Letters*, *36*, L06709. https://doi.org/10.1029/2009GL037593

Grise, K. M., Davis, S. M., Simpson, I. R., Waugh, D. W., Fu, Q., Allen, R. J., et al. (2019). Recent tropical expansion: Natural variability or forced response? *Journal of Climate*, *32*(5), 1551–1571.

Grise, K. M., Davis, S. M., Staten, P. W., & Adam, O. (2018). Regional and seasonal characteristics of the recent expansion of the tropics. *Journal of Climate*, *31*(17), 6839–6856.

Hawkins, E., & Sutton, R. (2012). Time of emergence of climate signals. *Geophysical Research Letters*, *39*, L01702. https://doi.org/10.1029/2011GL050087

Heffernan, O. (2016). The mystery of the expanding tropics. *Nature News*, *530*(7588), 20.

Hu, Y., & Fu, Q. (2007). Observed poleward expansion of the Hadley circulation since 1979. *Atmospheric Chemistry and Physics*, *7*(19), 5229–5236.
Hu, Y., & Zhou, C. (2010). Decadal changes in the Hadley circulation. *Advances in Geosciences*, *16*, 61.
Ilyina, T., Six, K. D., Segschneider, J., Maier-Reimer, E., Li, H., & Núñez-Riboni, I. (2013). Global ocean biogeochemistry model HAMOCC: Model architecture and performance as component of the MPI-Earth system model in different CMIP5 experimental realizations. *Journal of Advances in Modeling Earth Systems*, *5*, 287–315. https://doi.org/10.1029/2012MS000178
Johanson, C. M., & Fu, Q. (2009). Hadley cell widening: Model simulations versus observations. *Journal of Climate*, *22*(10), 2713–2725.
Jungclaus, J. H., Fischer, N., Haak, H., Lohmann, K., Marotzke, J., Matei, D., et al. (2013). Characteristics of the ocean simulations in the Max Planck Institute Ocean Model (MPIOM) the ocean component of the MPI-Earth system model. *Journal of Advances in Modeling Earth Systems*, *5*, 422–446. https://doi.org/10.1002/jame.20023
Kang, S. M., Deser, C., & Polvani, L. M. (2013). Uncertainty in climate change projections of the Hadley circulation: The role of internal variability. *Journal of Climate*, *26*(19), 7541–7554.
Liu, J., Song, M., Hu, Y., & Ren, X. (2012). Changes in the strength and width of the Hadley circulation since 1871. *Climate of the Past Discussions*, *8*(2), 695–713.
Lu, J. J., Vecchi, G. A., & Reichler, T. (2007). Expansion of the Hadley cell under global warming. *Geophysical Research Letters*, *34*, L06805. https://doi.org/10.1029/2006GL028443
Ma, J., Wang, H., & Zhang, Y. (2012). Will boreal winter precipitation over china increase in the future? An AGCM simulation under summer ice-free Arctic conditions. *Chinese Science Bulletin*, *57*(8), 921–926.
Maher, N., Milinski, S., Suarez-Gutierrez, L., Botzet, M., Dobrynin, M., Kornblueh, L., et al. (2019). The Max Planck Institute grand ensemble: Enabling the exploration of climate system variability. *Journal of Advances in Modeling Earth Systems*, *11*, 2050–2069. https://doi.org/10.1029/2019MS001639
Mariotti, A., Struglia, M. V., Zeng, N., & Lau, K. M. (2002). The hydrological cycle in the Mediterranean region and implications for the water budget of the Mediterranean sea. *Journal of Climate*, *15*(13), 1674–1690.
Nguyen, H., Evans, A., Lucas, C., Smith, I., & Timbal, B. (2013). The Hadley Circulation in reanalyses: Climatology, variability, and change. *Journal of Climate*, *26*(10), 3357–3376.
Nguyen, H., Hendon, H. H., Lim, E.-P., Boschat, G., Maloney, E., & Timbal, B. (2018). Variability of the extent of the Hadley circulation in the southern hemisphere: A regional perspective. *Climate Dynamics*, *50*(1-2), 129–142.
Nguyen, H., Lucas, C., Evans, A., Timbal, B., & Hanson, L. (2015). Expansion of the Southern Hemisphere Hadley cell in response to greenhouse gas forcing. *Journal of Climate*, *28*(20), 8067–8077.
Raiter, D., Galanti, E., & Kaspi, Y. (2020). The tropical atmospheric conveyor belt: A coupled Eulerian-Lagrangian analysis of the large-scale tropical circulation. *Geophysical Research Letters*, *47*, e2019GL086437. https://doi.org/10.1029/2019GL086437
Reick, C. H., Raddatz, T., Brovkin, V., & Gayler, V. (2013). Representation of natural and anthropogenic land cover change in MPI-ESM. *Journal of Advances in Modeling Earth Systems*, *5*, 459–482. https://doi.org/10.1002/jame.20022
Schwendike, J., Berry, G. J., Reeder, M. J., Jakob, C., Govekar, P., & Wardle, R. (2015). Trends in the local Hadley and local Walker circulations. *Journal of Geophysical Research: Atmospheres*, *120*, 7599–7618. https://doi.org/10.1002/2014JD022652
Schwendike, J., Govekar, P., Reeder, M. J., Wardle, R., Berry, G. J., & Jakob, C. (2014). Local partitioning of the overturning circulation in the tropics and the connection to the Hadley and Walker circulations. *Journal of Geophysical Research: Atmospheres*, *119*, 1322–1339. https://doi.org/10.1002/2013JD020742
Seager, R., Liu, H., Henderson, N., Simpson, I., Kelley, C., Shaw, T., et al. (2014). Causes of increasing aridification of the Mediterranean region in response to rising greenhouse gases. *Journal of Climate*, *27*(12), 4655–4676.
Seager, R., Naik, N., & Vecchi, G. A. (2010). Thermodynamic and dynamic mechanisms for large-scale changes in the hydrological cycle in response to global warming. *Journal of Climate*, *23*(17), 4651–4668.
Seager, R., Neelin, D., Simpson, I., Liu, H., Henderson, N., Shaw, T., et al. (2014). Dynamical and thermodynamical causes of large-scale changes in the hydrological cycle over North America in response to global warming. *Journal of Climate*, *27*(20), 7921–7948.
Seager, R., Ting, M., Held, I., Kushnir, Y., Lu, J., Vecchi, G., et al. (2007). Model projections of an imminent transition to a more arid climate in southwestern North America. *Science*, *316*(5828), 1181–1184.
Staten, P. W., Grise, K. M., Davis, S. M., Karnauskas, K., & Davis, N. (2019). Regional widening of tropical overturning: Forced change, natural variability, and recent trends. *Journal of Geophysical Research: Atmospheres*, *124*, 6104–6119. https://doi.org/10.1029/2018JD030100
Staten, P. W., Lu, J., Grise, K. M., Davis, S. M., & Birner, T. (2018). Re-examining tropical expansion. *Nature Climate Change*, *8*(9), 768.
Stevens, B. (2015). Rethinking the lower bound on aerosol radiative forcing. *Journal of Climate*, *28*(12), 4794–4819.
Stevens, B., Giorgetta, M., Esch, M., Mauritsen, T., Crueger, T., Rast, S., et al. (2013). Atmospheric component of the MPI-M earth system model: ECHAM6. *Journal of Advances in Modeling Earth Systems*, *5*, 146–172. https://doi.org/10.1002/jame.20015
Su, H., Jiang, J. H., Zhai, C., Shen, T. J., Neelin, J. D., Stephens, G. L., & Yung, Y. L. (2014). Weakening and strengthening structures in the Hadley Circulation change under global warming and implications for cloud response and climate sensitivity. *Journal of Geophysical Research: Atmospheres*, *119*, 5787–5805. https://doi.org/10.1002/2014JD021642
Tian, D., Guo, Y., & Dong, W. (2015). Future changes and uncertainties in temperature and precipitation over China based on CMIP5 models. *Advances in Atmospheric Sciences*, *32*(4), 487–496.
Waugh, D. W., Grise, K. M., Seviour, W. J. M., Davis, S. M., Davis, N., Adam, O., et al. (2018). Revisiting the relationship among metrics of tropical expansion. *Journal of Climate*, *31*(18), 7565–7581.